Transport calculations of the multiplicity moments for cylinders

NUCLEAR SCIENCE AND ENGINEERING

DOI: https://doi.org/10.1080/00295639.2021.1973178

Transport Calculation of the Multiplicity Moments for Cylinders

Imre Pázsit* and Victor Dykin

Chalmers University of Technology, Division of Subatomic, High Energy and Plasma Physics, Göteborg SE-412 96, Sweden

Received July 3, 2021
Accepted for Publication August 20, 2021

Abstract — *In a previous paper by Pázsit and Pál ["Multiplicity Theory Beyond the Point Model," Ann. Nucl. Energy, Vol. 154 (2021)], a general transport theory calculation of the factorial moments of the number of neutrons emitted spontaneously from a sample was elaborated. In contrast to the original derivations by Hage and Cifarelli ["On the Factorial Moments of the Neutron Multiplicity Distribution of Fission Cascades," Nucl. Instrum. Meth. Phys. Res. A, Vol. 236 (1985)] and Böhnel ["The Effect of Multiplication on the Quantitative Determination of Spontaneously Fissioning Isotopes by Neutron Correlation Analysis," Nucl. Sci. Eng., Vol. 90 (1985)], also referred to as the point model, in the transport model the spatial and angular dependence of the internal fission chain is taken into account with a one-speed transport theory treatment. Quantitative results were given for a spherical item, and the bias of the point model regarding the estimation of the fission rate as compared to the more exact space-dependent model was estimated as a function of the size of the sphere and the α factor.*

In the present paper the formalism and the quantitative work are extended to the treatment of items with cylindrical shapes, which are more relevant in many practical applications. Results are presented for both square cylinders ($D = H$) and for tall ($H/D > 1$) and flat ($H/D < 1$) cylinders. This way the differences between the cylinder and the sphere on one hand and those between the various cylinder shapes on the other hand can be estimated. The results show that the bias depends on the geometry of the cylinder quite moderately, but similarly to the case of the sphere, the bias of the point model is quite significant for larger item sizes and α values, and it is nonconservative (underestimates the fissile mass) as well.

Keywords — *Multiplicity counting, factorial moments, transport calculations, cylindrical item, collision number expansion.*

Note — *Some figures may be in color only in the electronic version.*

I. INTRODUCTION

The multiplicity moments (often referred to as the Böhnel moments) were calculated originally in the so-called point model,[1,2] in which the spatial transport and the energy degradation of the neutrons in the internal cascade are neglected. Application of the point model is naturally a simplification whose deficiencies have long been known.[3,4] On the other hand, it has the usual advantage of the simplified models, such as the infinite homogeneous system model of the Feynman-alpha and Rossi-alpha formulas for determining the subcritical reactivity; namely, it contains only the essential parameters, which are the matter of interest (the reactivity in the latter case) in a closed analytical form, and hence, it is well suited for diagnostic purposes, i.e., the extraction of the parameters of interest by an analytical inversion of the corresponding expressions.

With current computational resources, the multiplicity moments can be readily calculated for any sample composition and geometrical shape, including even

*E-mail: imre@chalmers.se

energy dependence, by a Monte Carlo simulation of the neutron transport and multiplication inside the item. Such calculations have a high fidelity in that they do not rely on any simplification of the physical process.[5,6] However, this methodology also shows the entailing difficulties: the numerical results depend on a large number of parameters in a fully quantitative manner, in which the effect of the important single parameter is concealed completely. Hence, the task of extracting the few parameters becomes rather complicated. Indeed, such calculations have been performed, but they simply show the results and the differences in comparison with the point model without giving a working recipe of how to utilize the results to extract the desired information.[3,4]

It is, however, possible to find a strategy by which the generality of the Monte Carlo method can be reduced and that yet supplies values of the multiplicity moments that are more realistic than those given by the point model. This is achieved by the extension of the master equation–based approach of the point model to the calculations of the multiplicity moments in one-speed transport theory. In this approach all aspects of the spatial transport of the neutrons are taken into account, although energy dependence is still neglected. This approach was currently developed and used to calculate the multiplicity moments in a spherical item.[7] The calculations showed the power of determining the multiplicity moments by deterministic methods (i.e., not by Monte Carlo simulations).

The purpose of the present paper is to extend the quantitative work for the calculation of the moments to an item with cylindrical shape. Naturally, this requires development of the formalism for cylindrical geometry. The motivation comes from the fact that a cylindrical shape is more realistic in practical cases. From the computational side this is a challenge since cylindrical geometry obeys fewer symmetry properties; hence, the formalism will include more variables. In contrast to the two-dimensional (2-D) phase space of the sphere (the radial and azimuthal variables), a cylindrical geometry has a four-dimensional phase space; i.e., one has to handle two more variables and perform correspondingly two more nested integrals in the collision number expansion used for the quantitative solution. From the methodology point of view, spheres have a simple shape characterized by only one single parameter (radius) whereas cylinders can have a different H/D ratio; i.e., they can be flat or square $(D = H)$ or have tall shapes. This way not only the difference between the sphere and a cylinder as such but also the difference among the different cylindrical geometries can be investigated.

II. GENERAL PRINCIPLES

Before turning to the calculation of the multiplicity moments for the cylinder, the general theory, valid for any sample shape, will be briefly summarized from Ref. 7. It is assumed that the only reaction for the source neutrons [spontaneous fission and (α, n) neutrons] is induced fission,[a] and we will use the neutron mean free path as the length unit (optical path units). Then, the probability distribution $p(\mathbf{n} = n|\boldsymbol{r}, \boldsymbol{\Omega})$ of the number $\mathbf{n}$ of neutrons leaving the sample due to one starting neutron with coordinates $(\boldsymbol{r}, \boldsymbol{\Omega})$ obeys the backward-type master equation,[b]

$$
\begin{aligned}
p(\mathbf{n} = n|\boldsymbol{r}, \boldsymbol{\Omega}) \equiv p(n|\boldsymbol{r}, \boldsymbol{\Omega}) &= e^{-\ell(\boldsymbol{r},\boldsymbol{\Omega})}\delta_{n,1} \\
&+ \int_0^{\ell(\boldsymbol{r},\boldsymbol{\Omega})} ds e^{-s} \sum_0^\infty p_{\boldsymbol{r}}(k) \sum_{n_1+n_2+\ldots+n_k=n} \int_{4\pi} \frac{d\boldsymbol{\Omega}_1}{4\pi}\frac{d\boldsymbol{\Omega}_2}{4\pi}\cdots\frac{d\boldsymbol{\Omega}_k}{4\pi} \\
&\times p(n_1|\boldsymbol{r}+s\boldsymbol{\Omega}, \boldsymbol{\Omega}_1) p(n_2|\boldsymbol{r}+s\boldsymbol{\Omega}, \boldsymbol{\Omega}_2)\ldots p(n_k|\boldsymbol{r}+s\boldsymbol{\Omega}, \boldsymbol{\Omega}_k)\,,
\end{aligned}
\tag{1}
$$

where $\ell(\boldsymbol{r}, \boldsymbol{\Omega})$ is the distance to the boundary of the item from $\boldsymbol{r}$ along $\boldsymbol{\Omega}$ in dimensionless optical path units and $p_r(k)$ is the probability distribution of the number of neutrons per induced fission.

Converting Eq. (1) to an equation for the generating function,

$$
g(z|\boldsymbol{r}, \boldsymbol{\Omega}) = \sum_{n=0}^\infty z^n p(n|\boldsymbol{r}, \boldsymbol{\Omega})\,,
\tag{2}
$$

one obtains a substantially more compact equation:

$$
\begin{aligned}
g(z|\boldsymbol{r}, \boldsymbol{\Omega}) &= z e^{-\ell(\boldsymbol{r},\boldsymbol{\Omega})} \\
&+ \int_0^{\ell(\boldsymbol{r},\boldsymbol{\Omega})} ds\, e^{-s} q_r\left(\frac{1}{4\pi}\int_{4\pi} d\boldsymbol{\Omega}'\, g(z|\boldsymbol{r}+s\boldsymbol{\Omega}, \boldsymbol{\Omega}')\right),
\end{aligned}
\tag{3}
$$

where $q_r(z)$ is the generating function of $p_r(k)$ and the quantity in the brackets is its argument.

Further, the number distribution $P(N|\mathbb{S})$ due to one source event $\mathbb{S}$ is given as

[a] Scattering and absorption can be included without significant complications, but they were neglected here for simplicity and transparency of the derivations.

[b] We use here the same convention as in Ref. 8; that is, a bold symbol like $\mathbf{n}$ stands for a random variable, and n is a concrete realization of it.

$$P(N|\mathbb{S}) = \frac{1}{V}\int_V dr \sum_0^\infty p_s(k) \sum_{N_1+N_2+\ldots+N_k=N} \int_{4\pi} \frac{d\boldsymbol{\Omega}_1}{4\pi}\frac{d\boldsymbol{\Omega}_2}{4\pi}\cdots\frac{d\boldsymbol{\Omega}_k}{4\pi} \times p(N_1|r,\boldsymbol{\Omega}_1)\,p(N_2|r,\boldsymbol{\Omega}_2)\ldots p(N_k|r,\boldsymbol{\Omega}_k), \tag{4}$$

where $p_s(k)$ is the number distribution of the source neutrons from spontaneous fission and (α, n) reactions. As is described in the literature,[7,9,10] $p_s(k)$ is the weighted average of the distribution $p_{sf}(k)$ of the number of neutrons from spontaneous fission and the distribution $\delta_{k,1}$ of the single neutrons emitted by (α, n) reactions. The weights are the relative intensities of the spontaneous fission and (α, n) reactions, the ratio of which is unknown in a given case, and it is one of the parameters to be determined by the multiplicity counting. It is customary to express this unknown ratio by the so-called α factor, which is defined as

$$\alpha = \frac{Q_\alpha}{F\,\nu_{sf,1}}\,, \tag{5}$$

where

Q_α = intensity of (α, n) reactions

F = intensity of the spontaneous fission events

$\nu_{sf,1}$ = expectation of the number of neutrons from spontaneous fission, i.e., the first moment of $p_{sf}(n)$.

The total intensity $Q = F + Q_\alpha$ of the source events is the sum of the respective intensities, which can be expressed by the definition of the α factor as

$$Q = F(1 + \alpha\nu_{sf,1})\,. \tag{6}$$

The generating function $G(z)$ of $P(N|\mathbb{S})$ obeys Eq. (7):

$$G(z) = \frac{1}{V}\int_V d\boldsymbol{r}\, q_s\left(\frac{1}{4\pi}\int_{4\pi} d\boldsymbol{\Omega} g(z|\boldsymbol{r},\boldsymbol{\Omega})\right), \tag{7}$$

where $q_s(z)$ is the generating function of the distribution $p_s(k)$ of the source neutrons, and similarly to Eq. (3), the quantity in the brackets is its argument.

Introducing the scalar (angularly integrated with respect to the direction of the starting neutron) single-particle–induced generating function,

$$g(z|\boldsymbol{r}) = \frac{1}{4\pi}\int_{4\pi} d\boldsymbol{\Omega} g(z|\boldsymbol{r},\boldsymbol{\Omega})\,, \tag{8}$$

one has

$$g(z|\boldsymbol{r}) = z g_0(z|\boldsymbol{r}) + \frac{1}{4\pi}\int_{4\pi} d\boldsymbol{\Omega}\int_0^{\ell(\boldsymbol{r},\boldsymbol{\Omega})} ds\, e^{-s} q_r[g(z|\boldsymbol{r}'(s))]\,, \tag{9}$$

where

$$g_0(z|\boldsymbol{r}) = \frac{1}{4\pi}\int_{4\pi} d\boldsymbol{\Omega}\, e^{-\ell(\boldsymbol{r},\boldsymbol{\Omega})} \tag{10}$$

and

$$r'(s) \equiv \boldsymbol{r} + s\boldsymbol{\Omega}\,. \tag{11}$$

In a similar way, the expression for the generating function of the source event–induced distribution reads as

$$G(z) = \frac{1}{V}\int_V d\boldsymbol{r}\, q_s[\,g(z|\boldsymbol{r})]\,. \tag{12}$$

It is seen from Eqs. (9) and (12) that for the calculation of the factorial moments of the source event–induced emissions, one does not need to calculate the angularly dependent generating functions; it is sufficient to know the scalar generating function. Further, only the single-particle–induced generating function (and hence its factorial moments) obeys an integral equation that has to be solved directly. In possession of these, the distribution of the source event–induced emissions is obtained by a simple quadrature. Hence, the computational burden is only associated with solving Eq. (9) for the factorial moments.

The factorial moments can be obtained by differentiating Eqs. (9) and (12) with respect to z, solving the arising integral equations for the moments of the single-neutron–induced distributions from Eq. (9), and integrating them in the expressions obtained from Eq. (12). These will not be given for the general case; they can be found in Ref. 7. They will be derived here for the particular case of a cylindrical item, which will be described in Sec. III.

III. EQUATIONS FOR CYLINDRICAL GEOMETRY

Let the radius of the cylinder be R and its height be H, measured in units of mean free path. In cylindrical

coordinates, the position of the neutron is defined by[c] $\boldsymbol{r} = \{r, \phi, h\}$, and its velocity direction is defined by $\boldsymbol{\Omega} = \{\mu, \varphi\}$, where $\mu = \cos\vartheta$, where ϑ is the polar angle. Because of the azimuthal symmetry of the cylindrical geometry, all quantities, such as the distribution $p(n|\boldsymbol{r}, \boldsymbol{\Omega})$ and hence also the generating functions $g(z|\boldsymbol{r}, \boldsymbol{\Omega})$ and $g(z|\boldsymbol{r})$ as well as their moments, will not depend on the azimuthal coordinate ϕ of the position vector. Hence, all quantities will depend on only the four variables $\{r, h, \mu, \varphi\}$.

Although the integrals in the equations derived from Eqs. (9) and (12) will be performed in cylindrical coordinates, calculating the radial and axial coordinates of $r'(s)$ of Eq. (1) and the distance $\ell(r, h, \mu, \varphi)$ to the boundary (the surface of the cylinder) is simpler with the help of Cartesian coordinates. Regarding the expression $\ell(r, h, \mu, \varphi)$ as a function of its arguments, one notes that the cylinder is defined through its boundaries as

$$x^2 + y^2 \le R^2 \quad \text{and} \quad 0 \le h \le H\,. \tag{13}$$

Because of the azimuthal symmetry, the starting point of the neutron can always lie at $y = 0$; hence, one has $x = r$. The Cartesian components of $\boldsymbol{\Omega}$ are given, as usual, as

$$\Omega_x = \sin\vartheta\cos\varphi = \sqrt{1-\mu^2}\cos\varphi\,, \tag{14}$$

$$\Omega_y = \sin\vartheta\sin\varphi = \sqrt{1-\mu^2}\sin\varphi\,, \tag{15}$$

and

$$\Omega_z = \cos\vartheta = \mu\,, \tag{16}$$

with $d\boldsymbol{\Omega} = d\mu d\varphi$. The Cartesian coordinates of $\boldsymbol{r}'(s)$ are given as

$$x'(s) = r + s\sqrt{1-\mu^2}\cos\varphi\,, \tag{17}$$

$$y'(s) = s\sqrt{1-\mu^2}\sin\varphi\,, \tag{18}$$

and

$$z'(s) = h + s\mu\,, \tag{19}$$

from which one obtains

$$r'(s) = \sqrt{x'(s)^2 + y'(s)^2} = \sqrt{r^2 + s^2(1-\mu^2) + 2rs\sqrt{1-\mu^2}\cos\varphi} \tag{20}$$

and

$$h'(s) = h + s\mu. \tag{21}$$

From the above, the distance $\ell(r, h, \mu, \varphi)$ to the boundary is found as the maximum value of s with which both conditions

$$r'(s) = \sqrt{r^2 + s^2(1-\mu^2) + 2rs\sqrt{1-\mu^2}\cos\varphi} \le R \tag{22}$$

and

$$0 \le h'(s) = h + s\mu \le H \tag{23}$$

are fulfilled. As soon as either of the above two inequalities is violated, it means that the path crossed either the side or the top/bottom of the cylinder. This value can be found as follows:

1. Find the positive roots s_1 and s_2, which are solutions of Eqs. (24) and (25):

$$r'(s_1) = R \tag{24}$$

and

$$\text{if } \mu < 0 : h'(s_2) = 0; \qquad \text{if } \mu > 0 : h'(s_2) = H. \tag{25}$$

2. If $\mu \neq 0$ and $\mu \neq \pm 1 \rightarrow \ell(r, h, \mu, \varphi) = \min(s_1, s_2)$.
   If $\mu = 0 \rightarrow \ell(r, h, \mu, \varphi) = s_1$.
   If $\mu = \pm 1 \rightarrow \ell(r, h, \mu, \varphi) = s_2$.

The roots of Eqs. (24) and (25) can be analytically calculated with the help of Eqs. (22) and (23). The first will be the root of the second-order algebraic equation,

$$s_1^2(1-\mu^2) + s_1 2r\sqrt{1-\mu^2}\cos\varphi + r^2 - R^2 = 0\,, \tag{26}$$

for the cases when

$$\mu \neq \pm 1\,. \tag{27}$$

[c] The axial coordinate of the position vector will be denoted by h to avoid confusion with the auxiliary variable z of the generating function.

When $\mu = \pm 1$, then s_1 will diverge, and s_2 will be the root that is equal to $\ell(r,h,\mu,\varphi)$. The second root is given as

$$\text{if } \mu < 0 : s_2 = -\frac{h}{\mu} \; ;$$
$$\text{if } \mu > 0 : s_2 = \frac{H-h}{\mu} \; . \tag{28}$$

Here again, for $\mu = 0, s_2$ diverges; hence, $\ell(r,h,\mu,\varphi) = s_1$.

With the above, everything is fixed for the concrete representation of Eqs. (9) and (12) in cylindrical geometry. The equation for the scalar generating function,

$$g(z|r,h) = \frac{1}{4\pi}\int_{-1}^{1} d\mu \int_0^{2\pi} d\varphi \, g(z|r,h,\mu,\varphi) \, , \tag{29}$$

of the single-neutron–induced distribution reads as

$$g(z|r,h) = z g_0(z|r,h) + \frac{1}{4\pi}\int_{-1}^{1} d\mu \int_0^{2\pi} d\varphi \int_0^{\ell(r,h,\mu,\varphi)} ds \, e^{-s} q_r[g(z|r'(s),h'(s))] \, , \tag{30}$$

with

$$g_0(z|r,h) = \frac{1}{4\pi}\int_{-1}^{1} d\mu \int_0^{2\pi} d\varphi \, e^{-\ell(r,h,\mu,\varphi)} \; . \tag{31}$$

The equation for the generating function of the source event–induced distribution is given as

$$G(z) = \frac{2}{R^2 H}\int_0^R r\,dr \int_0^H dh \, q_s[g(z|r,h)] \; . \tag{32}$$

III.A. Equations for the Moments

The equations for the moments can be derived by taking the derivatives of the generating functions $g(z|r,h)$ and $G(z)$ of Eqs. (30) and (32) at $z = 1$, respectively. The procedure goes exactly on the same lines as the corresponding derivation of the moments for a spherical item in Ref. 7; hence, the details of the derivations will not be given here. For consistency, the same notations will be used for the various moments as well as the conventions of Ref. 8 in that the first, second, and third factorial moments of the single-neutron–induced distribution will be denoted as $n(r,h)$, $m(r,h)$, and $w(r,h)$, respectively. These will read as

$$n(r,h) \equiv \langle \mathbf{n}(r,h) \rangle = \left. \frac{\partial \, g(z \mid r, \, h)}{\partial z} \right|_{z=1} , \tag{33}$$

$$m(r,h) \equiv \langle (\mathbf{n}(r,h)(\mathbf{n}(r,h)-1) \rangle = \left. \frac{\partial^2 g(z|r,h)}{\partial z^2} \right|_{z=1} , \tag{34}$$

and

$$w(r, \, h) \equiv \langle (\mathbf{n}(r, \, h)(\mathbf{n}(r, \, h)-1)(\mathbf{n}(r, \, h)-2) \rangle = \left. \frac{\partial^3 \, g(z \mid r, \, h)}{\partial \, z^3} \right|_{z=1} . \tag{35}$$

Likewise, the first three factorial moments of the source event–induced distribution will be denoted as N, M, and W. With these notations, the following Eqs. (36) through (44) are obtained for the moments.

First Moments

Single-neutron–induced expectation:

$$n(r,h) = n_0(r,h) + \frac{\nu_{r,1}}{4\pi}\int_{-1}^{1} d\mu \int_0^{2\pi} d\varphi \int_0^{\ell(r,h,\mu,\varphi)} ds \, e^{-s} n(r'(s),h'(s)) \; , \tag{36}$$

with

$$n_0(r,h) = \frac{1}{4\pi}\int_{-1}^{1} d\mu \int_0^{2\pi} d\varphi \, e^{-\ell(r,h,\mu,\varphi)} \, . \tag{37}$$

Source event–induced expectation:

$$N = \frac{2\nu_{s,1}}{R^2 H}\int_0^R r\,dr \int_0^H dh \, n(r,h) \, . \tag{38}$$

Second Moments

$$m(r,h) = A(r,h) + \frac{\nu_{r,1}}{4\pi}\int_{-1}^{1} d\mu \int_0^{2\pi} d\varphi \int_0^{\ell(r,h,\mu,\varphi)} ds \, e^{-s} m(r'(s),h'(s)) \, , \tag{39}$$

with

$$A(r,h) = \frac{\nu_{r,2}}{4\pi}\int_{-1}^{1} d\mu \int_0^{2\pi} d\varphi \int_0^{\ell(r,h,\mu,\varphi)} ds \, e^{-s} n^2(r'(s),h'(s)) \tag{40}$$

and

$$M = \frac{2}{R^2 H}\int_0^R r\,dr \int_0^H dh\left\{\nu_{s,2}\, n^2(r,h) + \nu_{s,1}\, m(r,h)\right\} . \tag{41}$$

Third Moments

$$w(r,h) = B(r,h) + \frac{\nu_{r,1}}{4\pi}\int_{-1}^{1} d\mu \int_0^{2\pi} d\varphi \int_0^{\ell(r,h,\mu,\varphi)} ds\, e^{-s}\, w(r'(s), h'(s)) , \tag{42}$$

with

$$B(r,h) = \frac{1}{4\pi}\int_{-1}^{1} d\mu \int_0^{2\pi} d\varphi \int_0^{\ell(r,h,\mu,\varphi)} ds e^{-s}\{\nu_{r,3} n^3(r'(s), h's)) + 3\nu_{r,2} n(r'(s), h'(s)) m(r'(s), h'(s))\} \tag{43}$$

and

$$W = \frac{2}{R^2 H}\int_0^R r dr \int_0^H dh\left\{\nu_{s,3}\, n^3(r,h) + 3\,\nu_{s,2}\, n\,(r,h)\; m\,(r,h) + \nu_{s,1}\, w\,(r,h)\right\} . \tag{44}$$

In the following, the above expressions for the factorial moments, Eqs. (36) though (44), will be evaluated quantitatively for a particular item with given material composition and varying size. The solution method is described in Sec. IV, and the quantitative results together with a comparison with that of the point model are given in Sec. V.

IV. NUMERICAL SOLUTION

As mentioned earlier, only the single-neutron–induced moments need to be determined from an integral equation; the source event–induced moments can be obtained from the former by simple integration. Similarly to Ref. 7, these equations will be solved numerically by a collision number (i.e., Neumann series) expansion.[11] The procedure goes along the same lines as for the sphere except that because of the reduced symmetry in the case of the cylinder, the iterations require the execution of more nested integrals. This will make the computational burden significantly higher than for the sphere.

The procedure will be outlined here for the first moment only; it is the same for the higher-order moments. Thus, taking the uncollided part $n_0(r,h)$ of Eq. (37) as the starting (zeroth) term of the expansion, the next term $n_1(r,h)$, which is the expectation of the number of neutrons that leave the cylinder after the first collision, will be given as

$$n_1(r,h) = \frac{\nu_{r,1}}{4\pi}\int_{-1}^{1} d\mu \int_0^{2\pi} d\varphi \int_0^{\ell(r,h,\mu,\varphi)} ds\, e^{-s}\, n_0(r'(s), h'(s)) , \tag{45}$$

and in general, the k'th term, the contribution from neutrons having collided exactly k times, is given as

$$n_k(r,h) = \frac{\nu_{r,1}}{4\pi}\int_{-1}^{1} d\mu \int_0^{2\pi} d\varphi \int_0^{\ell(r,h,\mu,\varphi)} ds\, e^{-s} n_{k-1}(r'(s), h'(s)) . \tag{46}$$

The full solution is obtained by summing up the contributions for all collision numbers:

$$n(r,h) = \sum_{k=0}^{\infty} n_k(r,h) . \tag{47}$$

Having obtained $n(r,h)$, it can be used in Eq. (38) to calculate the source event–induced expectation N.

The procedure is the same for the higher-order moments. The only difference is that the $A(r,h)$ and $B(r,h)$ of Eqs. (40) and (43), respectively, will replace $n_0(r,h)$ as the starting term of the iteration. Since $A(r,h)$ contains $n(r,h)$ and since $B(r,h)$ contains both $n(r,h)$ and $m(r,h)$, the moment equations have to be solved sequentially, starting from the lowest-order moments.

A comparison shows that for the cylinder, generation of each term of the iteration requires the calculation of a threefold integral as compared to the twofold integral in the case of a sphere. This is because for the cylinder, there is an additional integration with respect to the azimuthal variable φ. Besides, whereas the scalar expectation $n(x)$ (x being the radial coordinate in optical units) for the sphere had to be calculated on a one-dimensional grid of x_i points, here, $n(r,h)$ has to be calculated on a 2-D grid of r_i, h_j points. Hence, roughly, the computational demand for the cylinder is $N_h \cdot N_\varphi$ times larger than for the sphere. Typical values of the grid points are $N_h = N_\varphi = 100$; thus, the calculations take about 10^4 times longer than for the sphere.

For the calculations, the high-performance clusters VERA and Tetralith of the Swedish National Infrastructure for Computing (SNIC) were used. Whereas the calculations for the sphere in Ref. 7 were performed by Mathematica, the present calculations were made by Matlab.

V. QUANTITATIVE ANALYSIS AND COMPARISON WITH THE POINT MODEL

The numerical work again will go along the same lines as in our previous paper for the sphere.[7] For the sake of easy comparison between the sphere and the cylinder, the same material composition of the item and corresponding factorial moments of the spontaneous and induced fission from Ref. 6 will be used, and the same two cases $\alpha = 0$ and $\alpha = 0.5$ will be considered, where the factor α expressing the fraction of the mean number of neutrons generated in (α, n) reactions is defined in Eq. (5). As in the previous work, it is assumed that the presence of light atomic number materials in the case of $\alpha = 0.5$ does not affect the statistics of the spontaneous and induced fission neutrons. The factorial moments of the source and induced fission neutron numbers for the two α values are shown in Table I.

Regarding the quantitative analysis, it will be more extensive than in the case of the sphere. In the latter case, the mass of the item was determined by the only geometrical parameter, i.e., the radius R of the sphere. In the present case, the situation is more involved due to the cylinder having two parameters, its height H and diameter $D = 2R$. Cylinders of the same volume (mass) can have different shapes with different H/D ratios (= aspect ratios), which also has an effect on the results.

In order to simplify and structure the presentation of the quantitative work such that the dependence of the results on both the mass (volume) of the item as well as its shape could be discerned, we selected to present results for three characteristic cases (shapes): a square cylinder ($H/D = 1$), a long cylinder ($H/D = 2.5$), and a flat cylinder ($H/D = 0.2$). Calculations were made for all three shapes by changing the radius, with the shape (aspect ratio H/D) being unchanged. For each shape, the dependence of the first three factorial moments of the source event–induced number distribution will be shown, as for the sphere in Ref. 7. However, since the same radii for the three shapes would correspond to different masses (volumes), in order for a correct comparison of the results, these will be plotted as a function of the so-called effective radius R_{eff}. This latter is defined as the radius of an equivalent square cylinder with the same volume as the actual long and flat cylinders, respectively. In the formula, one has

$$R_{eff} = R\left(\frac{H}{D}\right)^{\frac{1}{3}} , \tag{48}$$

where R is the actual radius of the cylinder and H/D is the fixed aspect ratio of the particular shape. Obviously, for a square cylinder, one has $R_{eff} = R$ whereas for the long and the flat cylinders, one has $R_{eff} > R$ and $R_{eff} < R$, respectively.

Before turning to the quantitative work, there is one more point to consider. Similarly to the discussion in Ref. 7, the results will be compared with those of the point model. For a correct comparison of the results of the space-dependent transport theory results with those of the point model, the first collision probability must be the same for both models. To this order, the first collision probability p is needed for each particular cylinder geometry. This was easy to obtain in the case of spherical geometry since a simple analytic expression exists for the first collision probability as a function of the radius of the sphere.[12,13] For cylinders, there also exists an analytical expression,[14] but it is rather complicated, and it contains singular integrals.

Therefore, a direct numerical calculation was found to be much simpler. One notes that the average escape probability p_{esc} of neutrons for the case of a homogeneously distributed isotropic source is equal to

$$p_{esc} = \frac{1}{V}\int_V d\boldsymbol{r} n_0(\boldsymbol{r}) , \tag{49}$$

where $n_0(\boldsymbol{r})$ is shorthand for the uncollided term, Eq. (37). Hence, the first collision probability p is equal to

$$p = 1 - p_{esc} = 1 - \frac{1}{V}\int_V d\boldsymbol{r} n_0(\boldsymbol{r}) , \tag{50}$$

TABLE I

The First Three Factorial Moments of Spontaneous and Induced Fission and Those of a Source Event with $\alpha = 0.5$ in a Sample of 20 wt% ^{240}Pu and 80 wt% ^{239}Pu

Type of Source Event	First Moments	Second Moments	Third Moments
Spontaneous fission	$\nu_{sf,1} = 2.1538$	$\nu_{sf,2} = 3.7912$	$\nu_{sf,3} = 5.2146$
Source event with $\alpha = 0.5$	$\nu_{s,1} = 1.5554$	$\nu_{s,2} = 1.8254$	$\nu_{s,3} = 2.5108$
Induced fission	$\nu_{r,1} = 3.135$	$\nu_{r,2} = 8.1162$	$\nu_{r,3} = 17.0028$

which for cylindrical geometry using Eq. (37) leads to

$$p = 1 - \frac{1}{2\pi R^2 H}\int_0^R r\,dr\int_0^H dh\int_{-1}^{1} d\mu\int_0^{2\pi} d\varphi\, e^{-\ell(r,h,\mu,\varphi)} \quad . \tag{51}$$

This formula can be easily evaluated numerically. The first collision probability will be calculated by this formula when the results of the transport theory calculations are compared with the results of the point model.

The dependence of the first collision probability p on the effective radius for the three chosen cylinder shapes is shown in Fig. 1. It is seen from Fig. 1 that the smooth shapes of the dependence of the first collision probability on the effective radii are similar to each other and also quite similar in shape to that of the sphere.[15] It is also seen that for the same effective radius, it is the largest for the square cylinder (aspect ratio $H/D = 1$) and the smallest for the flat cylinder. This might appear obvious since for the same effective radius, the square cylinder has the minimum surface (maximum volume/surface ratio) and in reactor physics terms is expected to have the least leakage and hence the largest k_{eff}.

However, as it was pointed out by van Dam[16] and Arzhanov,[17] despite what intuition would suggest, the minimum of the volume/surface ratio (aspect ratio = 1) for an item does not result in the maximum of the k_{eff} or minimum of the leakage. The situation is the same for the first collision probability, as is illustrated in Fig. 2, which shows the dependence of the first collision probability p on the aspect ratio H/D for three different effective radii.

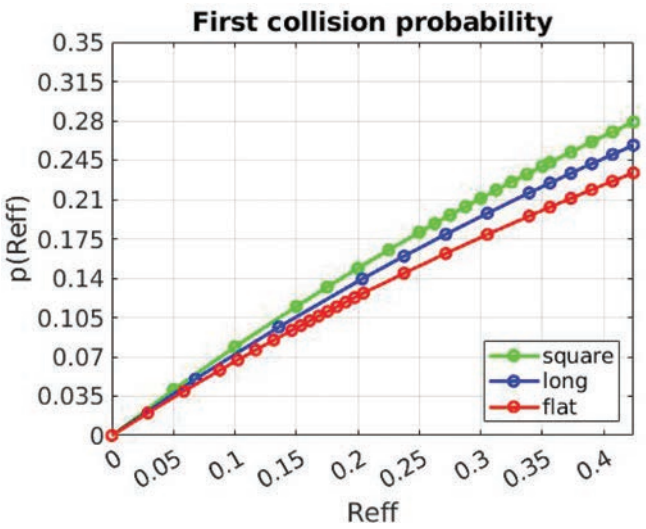

Fig. 1. First collision probability as function of cylinder effective radius R_{eff} for the square ($H = D$), long ($H/D = 2.5$), and flat ($H = 0.2D$) cylinders.

Figure 2 shows that for all three cases the maximum of the first collision probability p is at an aspect ratio $H/D < 1$. The exact values of H/D that yield the maximum of p for the three different cases are not easily seen in Fig. 2. As Table II shows, the aspect ratio yielding the maximum of p is at $H/D = 0.88$ for all three effective radii, indicating that the position of the maximum does not depend on the volume of the cylinder. It is worth noting that this value of the aspect ratio is not the same as the $H/D = 0.924$ given by van Dam[16] for the aspect ratio yielding the maximum of k_{eff} of a homogeneous cylinder in diffusion theory. However, they both deviate from the ratio $H/D = 1$ into the same direction (less than unity aspect ratio), showing a consistency. The reason for the difference in the actual value is understandable in view of the fact that the k_{eff} does not solely depend on the first collision probability but also depends on the higher-order collision probabilities, which differ from p. Also, the calculation of the k_{eff} of a homogeneous cylinder in

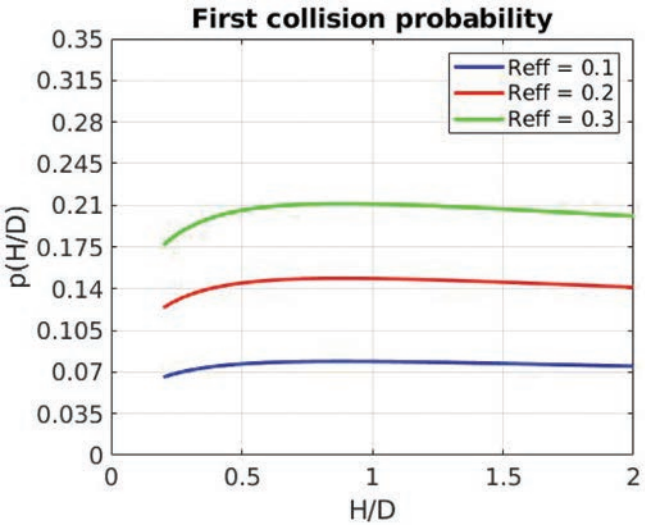

Fig. 2. First collision probability as function of the aspect ratio H/D for three different cylinder effective radii $R_{eff} = 0.1, 0.2, \text{and} 0.3,$ respectively.

TABLE II

The Maximum Value of First Collision Probability as Function of Cylinder Geometry $\frac{H}{D}$ for Different Cylinder Effective Radii

Cylinder Effective Radius, R_{eff}	H/D	Maximum p_1
$R_{eff} = 0.1$	0.88	0.079
$R_{eff} = 0.2$	0.88	0.149
$R_{eff} = 0.3$	0.88	0.2112

Ref. 16 is based on diffusion theory whereas our calculations here are based on transport theory.

With these preliminaries, everything is available for the quantitative analysis of the moments of the number of emitted particles per source event.

V.A. First Moments

The dependence of the mean values (first factorial moments) on the radius (in optical units) of a square cylinder $R = R_{eff}$ is shown in Fig. 3 for both the point model and the space-dependent model for the cases $\alpha = 0$ (Fig. 3a) and $\alpha = 0.5$ (Fig. 3b). The tendencies are very similar to those observed for the sphere. For obvious reasons, which are independent of the geometry, for very small values of R, the point model and space-dependent model values are both equal to the mean values of source emission particles for both values of α. As Table I shows, this value is smaller for the case $\alpha = 0.5$, and hence, the values of the first moment remain systematically lower than those for $\alpha = 0$ for all values of R_{eff}. With increasing radius, the mean values of both the point model and the space-dependent model start to increase, and similarly to the case of the sphere, the mean values by the space-dependent model increase faster than those by the point model. The difference increases with increasing radius. The quantitative values are of course different from those of the sphere; among others, they are larger for the cylinder than for the sphere with the same radius for the simple reason that a cylinder with the same radius has a larger volume (mass) than the sphere.

The dependence of the mean values predicted by the point model and the space-dependent model for $\alpha = 0$ and $\alpha = 0.5$ for the long and the flat cylinders is shown as a function of the effective radius in Figs. 4 and 5, respectively. These are again similar in character to both the square cylinder and the sphere. Although it is not well seen in Figs. 4 and 5, they all start at $R = 0$ from the same values since these values are geometry independent. The values predicted by the space-dependent model here again increase faster with increasing effective radius than those by the point model, but the

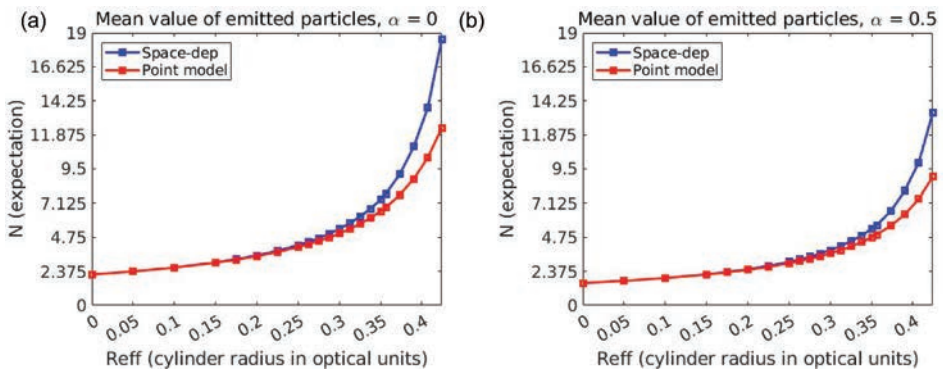

Fig. 3. Mean value of emitted particles as function of cylinder effective radius for square cylinder, $H = D$ for the cases (a) $\alpha = 0$ and (b) $\alpha = 0.5$.

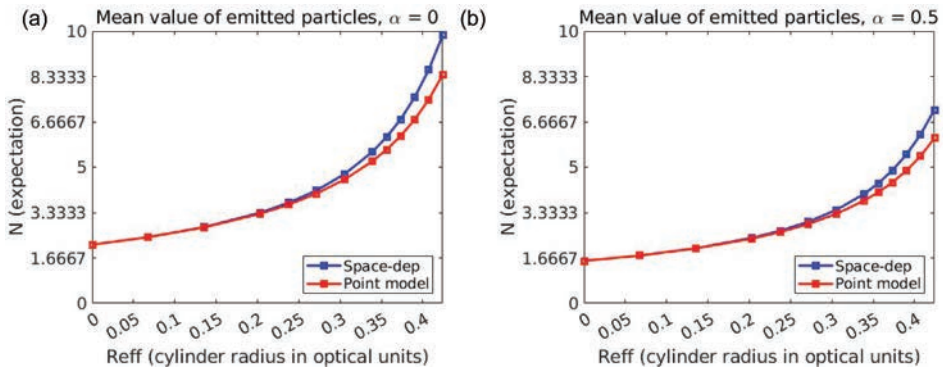

Fig. 4. Mean value of emitted particles as function of cylinder effective radius for (a) $\alpha = 0$ and (b) $\alpha = 0.5$, long cylinder, $H/D = 2.5$.

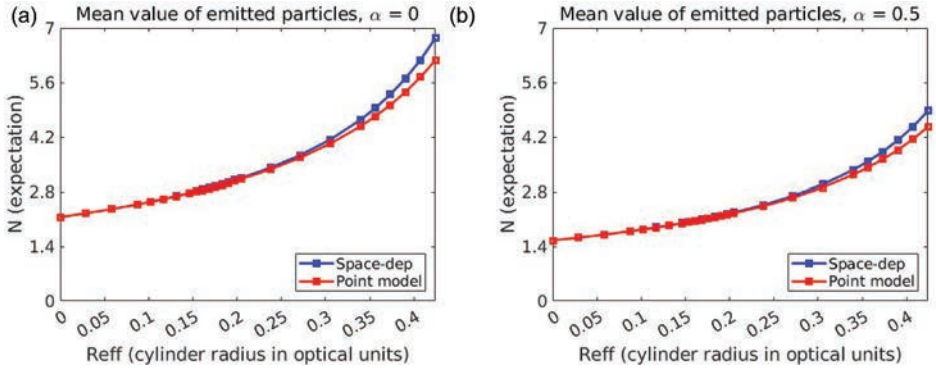

Fig. 5. Mean value of emitted particles as function of cylinder effective radius for (a) α = 0 and (b) α = 0.5, flat cylinder, $H/D = 0.2$.

rates of the rise are different from each other and from that of the square cylinder. For both the long cylinder and the flat cylinder, at the same effective radius, the mean values are lower than those of the square cylinder; the values from the long cylinder are larger than those of the flat cylinder. This is in agreement with Fig. 1, which shows that for the shapes investigated here, for a given effective radius the first collision probability is the largest for the square cylinder and the smallest for the flat cylinder.

V.B. Second Moments

Quantitative values for the second factorial moments (doubles) for the square, long, and flat cylinders are shown in Figs. 6, 7, and 8, respectively. As expected, the same tendencies as well as similarities and differences can be observed for the second moments as for the first moments. As for the sphere, the differences between the space-dependent and point model values became larger with increasing effective radius. In addition, the differences between the second moments corresponding to the various shapes are also larger than for the first moment, again those corresponding the square cylinder being the largest and those of the flat cylinder being the smallest.

V.C. Third Moments

The quantitative values for the third factorial moments (triples) for the square, long, and flat cylinders are shown in Figs. 9, 10, and 11, respectively. As could be expected, the trends observed in the foregoing Figs. (3) through (8) continue. The third moments themselves and the differences between both the space-dependent and point model values as well as those between the cylinders with different shapes increase even faster with increasing radius than for the first and second moments. At $R_{eff} = 0.3$, for the square cylinder, the difference between the space-dependent model and the point model exceeds 50% considerably. Actually, because of the intense internal multiplication and hence several collisions before the neutrons leave the item, for such values of R_{eff}, the calculations of the higher moments with the collision number expansion become

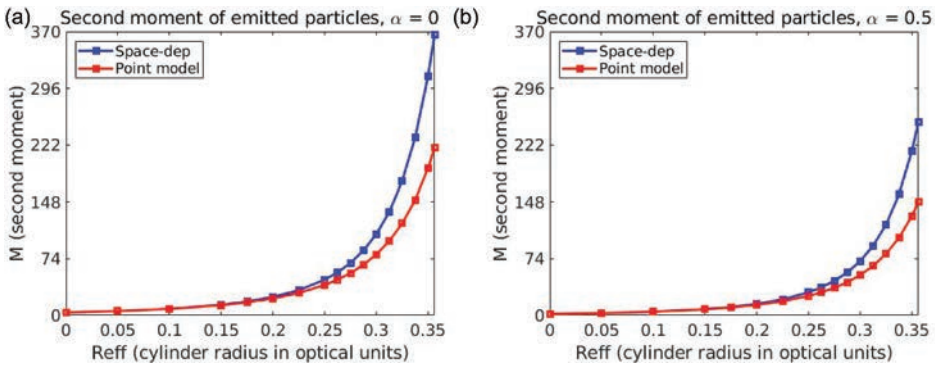

Fig. 6. Second moment of emitted particles as function of cylinder effective radius for (a) α = 0 and (b) α = 0.5, square cylinder, $H = D$.

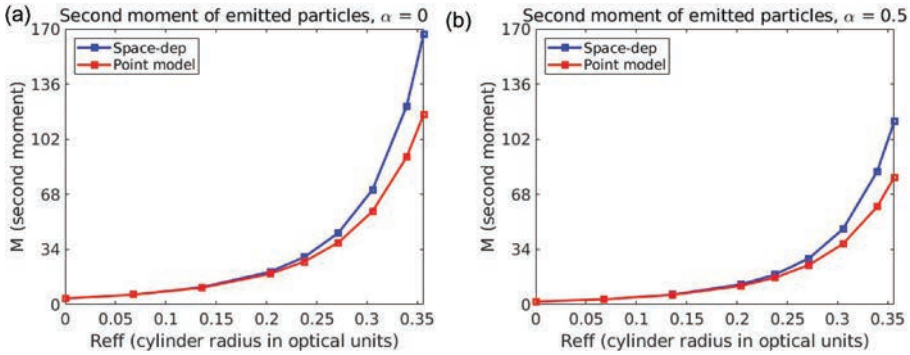

Fig. 7. Second moment of emitted particles as function of cylinder effective radius for (a) $\alpha = 0$ and (b) $\alpha = 0.5$, long cylinder, $H/D = 2.5$.

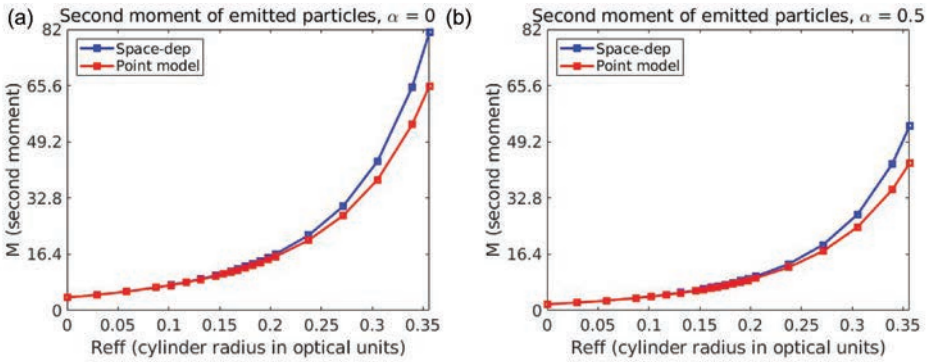

Fig. 8. Second moment of emitted particles as function of cylinder effective radius for (a) $\alpha = 0$ and (b) $\alpha = 0.5$, flat cylinder, $H/D = 0.2$.

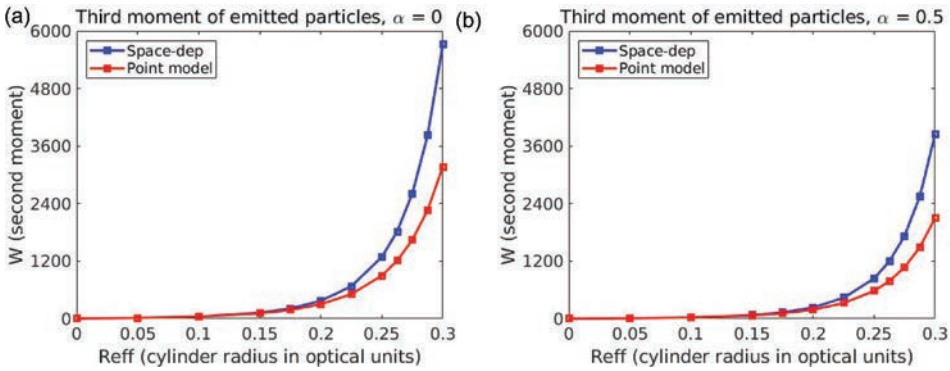

Fig. 9. Third moment of emitted particles as function of cylinder effective radius for (a) $\alpha = 0$ and (b) $\alpha = 0.5$, square cylinder, $H = D$.

computationally rather demanding, requiring long running times.

The reason for the space-dependent model predicting higher values for all the moments was analyzed for the sphere in Ref. 7, and the same is valid for the cylinder. Namely, the space-dependent model predicts a larger internal multiplication and hence also a larger leakage multiplication than the point model.

V.D. The Bias of the Point Model

It is worth investigating what effect the difference in the space-dependent and point model values has on the accuracy on the determination of the fissile mass of the item, which is the main purpose of multiplicity counting. On the assumption that the space-dependent moments, based on one-speed transport theory, give a better

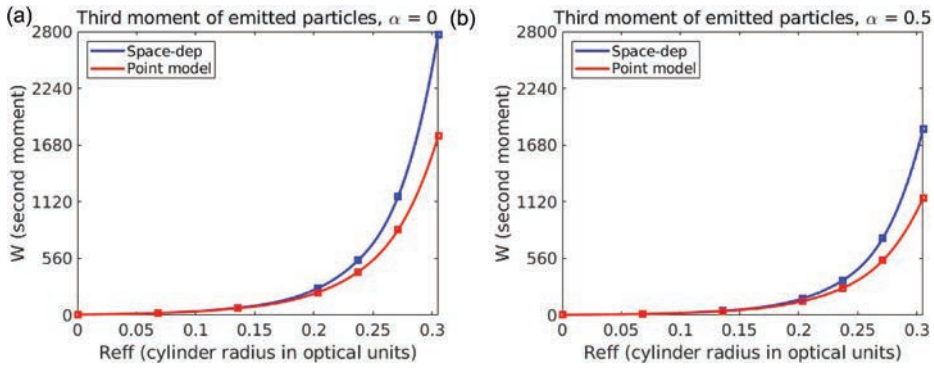

Fig. 10. Third moment of emitted particles as function of cylinder effective radius for (a) α = 0 and (b) α = 0.5, long cylinder, H/D = 2.5.

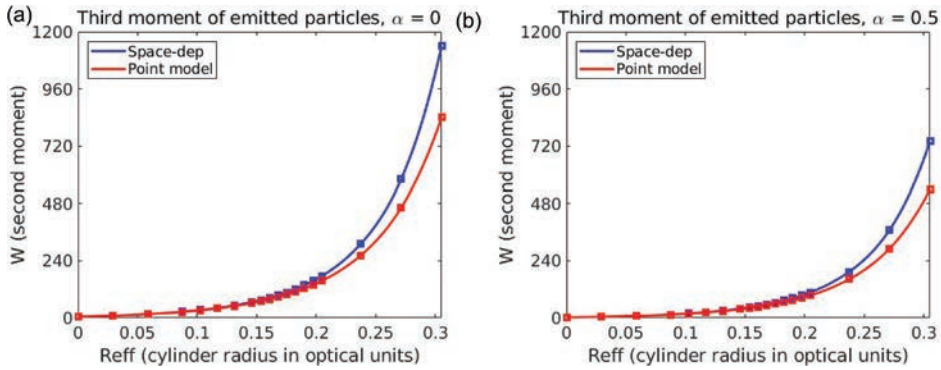

Fig. 11. Third moment of emitted particles as function of cylinder effective radius for (a) α = 0 and (b) α = 0.5, flat cylinder, H/D = 0.2.

estimation of the factorial moments than the point model, the former can be accepted as the true values. Then, using the point model formulas for the unfolding of the fission rate when the measured multiplicity rates (i.e., those given by the space-dependent model) do not correspond to those given by the point model for the same fission rate will lead to a bias in the estimation of the fission rate. In possession of the point model formulas and hence the numerical values of the singles, doubles, and triples rates, as well as the numerical values of the factorial moments given by the space-dependent model for the same material properties and fission rate, the bias can be quantified.

The procedure is described in detail in Ref. 7 in connection with the calculation of the moments for the sphere in the space-dependent model; hence, only a brief summary is given here. First, the factorial moments need to be converted into multiplicity rates (singles, doubles and triples rates) by introducing the fission rate F of ^{240}Pu. With the factorial moments N, M, and W, these are given by

$$S_{sp} = F\,(1 + \alpha \nu_{sf,1})\,\varepsilon N\,, \tag{52}$$

$$D_{sp} = \frac{F\,(1 + \alpha \nu_{sf,1})\,\varepsilon^2 f_d}{2}\,M\,, \tag{53}$$

and

$$T_{sp} = \frac{F\,(1 + \alpha \nu_{sf,1})\,\varepsilon^3 f_t}{6}\,W\,, \tag{54}$$

where ε is the detector efficiency and f_d and f_t are the so-called doubles and triples gate factors, respectively.[9,10] The actual values of all of these factors do not affect the bias since they appear in both the point model and the space-dependent model exactly the same way. Hence, they can be assumed to be unity in the quantitative work. They have been given here only for completeness and easy identification with the literature.

On the other hand, because in the point model the factorial moments and hence also the corresponding S, D, and T rates are analytical functions of the fission rate, the factorial moments of the spontaneous and induced fission, and that of the α factor, the fission rate can be expressed by

an inversion of these formulas. This is done by determining first the so-called leakage multiplication **M** (Refs. 9 and 10) from a third-order algebraic equation, which reads as

$$a + b\mathbf{M} + c\mathbf{M}^2 + \mathbf{M}^3 = 0\,, \tag{55}$$

with

$$a = \frac{-6\boldsymbol{T}\nu_{sf,2}(\nu_{r,1}-1)}{\varepsilon^2 f_t \boldsymbol{S}\left[\nu_{sf,2}\nu_{r,3}-\nu_{sf,3}\nu_{r,2}\right]}\,, \tag{56}$$

$$b = \frac{2\boldsymbol{D}\left[\nu_{sf,3}(\nu_{r,1}-1)-3\nu_{r,2}\nu_{sf,2}\right]}{\varepsilon f_d \boldsymbol{S}\left[\nu_{sf,2}\nu_{r,3}-\nu_{sf,3}\nu_{r,2}\right]}\,, \tag{57}$$

and

$$c = \frac{6\nu_{r,2}\nu_{sf,2}\boldsymbol{D}}{\varepsilon f_d \boldsymbol{S}\left[\nu_{sf,2}\nu_{r,3}-\nu_{sf,3}\nu_{r,2}\right]} - 1\,, \tag{58}$$

where the boldface notation of the multiplicity rates is meant to indicate that in an application, these are taken from the measurement and not from the theory. In possession of **M**, the fission rate is obtained as

$$F \equiv F_{point} = \frac{\left[\dfrac{2\boldsymbol{D}}{\varepsilon f_d} - \dfrac{\mathbf{M}(\mathbf{M}-1)\nu_{r,2}\boldsymbol{S}}{\nu_{r,1}-1}\right]}{\varepsilon\,\mathbf{M}^2\nu_{sf,2}}\,. \tag{59}$$

The bias can then be estimated as follows. One substitutes the values S_{sp}, D_{sp}, and T_{sp} of Eqs. (52), (53), and (54) for S, D, and T in Eqs. (56), (57), and (58) and then uses the **M** so obtained from Eq. (55) in Eq. (59) to obtain F_{point}. The bias $\mathbb{C}$ is then given as

$$\mathbb{C} = \frac{F_{point}}{F}\,. \tag{60}$$

The bias of the point model was calculated according to the above procedure for the three cylinder shapes and for the cases $\alpha = 0$ and $\alpha = 0.5$. The results are shown in Fig. 12. Once again, the results show a considerable resemblance to those by the sphere. The bias is nonconservative; i.e., the application of the point model leads to an underestimation of the fissile mass, and this underestimation increases with the fissile mass. Moreover, it is considerably larger for the case $\alpha = 0.5$ than for $\alpha = 0$. As is mentioned in Ref. 7, these results are also consistent with other studies of the bias of the point model.[3]

The reasons for the bias, and in particular the underestimation of the fission rate, are also discussed in Ref. 7, and the considerations are also valid for the results here. In essence, the underestimation could be lead back to the fact that the third moment by the space-dependent model exceeds that of the point model more significantly than for the first moment. This fact can also be observed in the results for the cylinder, shown in this paper.

VI. CONCLUSIONS

An earlier work concerning the calculation of the multiplicity moments from a sample containing fissionable and fissile material with one-speed transport theory for a spherical item was extended to cylinders. Equations were derived for the first three factorial moments of the number of neutrons emitted from the sample by one source event (spontaneous fission), and they were solved numerically by a collision number expansion method. In addition to the study of the dependence of the moments on the size of the sample, the influence of the shape of the cylindrical item also was investigated. Three characteristic cases, i.e., a square,

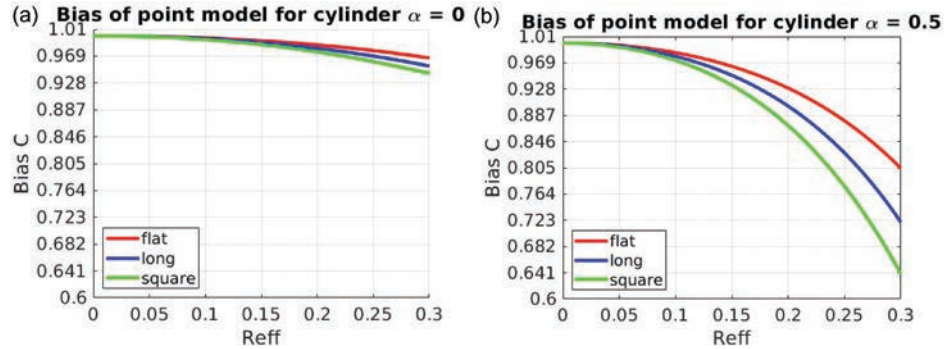

Fig. 12. Bias between the point and the space-dependent models as function of cylinder effective radius R_{eff} for (a) $\alpha = 0$ and (b) $\alpha = 0.5$.

a long cylinder, and a flat cylinder, were investigated quantitatively, and the bias of the point model was evaluated.

It was found that the results showed considerable resemblance to those obtained for the sphere regarding both tendencies and quantitative values. The deviation of the results from those obtained for a sphere as well as among the various cylinder shapes could be quantified. The quantitative differences are relatively modest; however, in many practical cases one has to handle cylindrical items, for which the present work supplies better estimates than the point model, or the space-dependent values calculated for a sphere.

One might also ask how the results presented in this paper can be used in practical applications to unfold the unknown fissile mass instead of using the biased point model formulas. This is not completely trivial since unlike in the case of the point model, the moments and hence also the multiplicity rates are not given by simple closed analytical formulas, and hence, an analytical inversion similar to that given in Eqs. (55) through (59) is not available. As is described in Ref. 7, for the case when $\alpha = 0$, i.e., pure metallic items, a simple correction factor can be given to reconstruct the true fission rate from the biased one obtained from the point model. In the case when $\alpha \neq 0$, such a simple procedure is not available since the unfolding of the true fission rate requires multivariate fitting techniques. As is also mentioned in Ref. 7, one possibility is to use machine learning methods similar to those used for the inversion of the joint neutron-gamma measurements,[18] for which training data can be generated by the method demonstrated in this paper. Such a possibility will be explored in future work.

Acknowledgments

The computations presented in this paper were enabled by resources provided by the SNIC at the Chalmers Centre for Computational Science and Engineering (C3SE), and at the National Supercomputer Centre, Linköping University (LiU), partially funded by the Swedish Research Council through grant agreement number 2018-05973. Mikael Öhman at C3SE and Weine Olovsson at LiU are acknowledged for assistance concerning technical and implementational aspects in making the code run on the SNIC resources. The authors also want to thank the two anonymous reviewers for their kind comments.

ORCID

Imre Pázsit http://orcid.org/0000-0001-7445-1697
Victor Dykin http://orcid.org/0000-0002-2751-8614

References

1. W. HAGE and D. M. CIFARELLI, "On the Factorial Moments of the Neutron Multiplicity Distribution of Fission Cascades," *Nucl. Instrum. Meth. Phys. Res. A*, **236**, *1*, 165 (1985); https://doi.org/10.1016/0168-9002(85)90142-1.
2. K. BÖHNEL, "The Effect of Multiplication on the Quantitative Determination of Spontaneously Fissioning Isotopes by Neutron Correlation Analysis," *Nucl. Sci. Eng.*, **90**, *1*, 75 (1985); https://doi.org/10.13182/NSE85-2.
3. J. M. BURWARD-HOY et al., "Achieving Accurate Neutron-Multiplicity Analysis of Metals and Oxides with Weighted Point Model Equations," *Proc. 45th INMM Annual Mtg.*, Orlando, Florida, July 18–22, 2004, Institute of Nuclear Materials Management (2004).
4. S. CROFT et al., "An Alternative Perspective on the Weighted Point Model for Passive Neutron Multiplicity Counting," *Proc. 48th INMM Annual Mtg.*, Tucson, Arizona, July 8–12, 2007, Institute of Nuclear Materials Management (2007).
5. S. A. POZZI et al., "MCNPX-PoliMi for Nuclear Nonproliferation Applications," *Nucl. Instrum. Meth Phys. Res. A*, **694**, 119 (2012); https://doi.org/10.1016/j.nima.2012.07.040.
6. A. ENQVIST, I. PÁZSIT, and S. POZZI, "The Number Distribution of Neutrons and Gamma Photons Generated in a Multiplying Sample," *Nucl. Instrum. Meth. Phys. Res. A*, **566**, *2*, 598 (2006); https://doi.org/10.1016/j.nima.2006.06.046.
7. I. PÁZSIT and L. PÁL, "Multiplicity Theory Beyond the Point Model," *Ann. Nucl. Energy*, **154**, 108119 (2021); https://doi.org/10.1016/j.anucene.2020.108119.
8. I. PÁZSIT and L. PÁL, *Neutron Fluctuations: A Treatise on the Physics of Branching Processes*, Elsevier (2008).
9. N. ENSSLIN et al., "Application Guide to Neutron Multiplicity Counting," LA-13422-M, Los Alamos National Laboratory (1998).
10. I. PÁZSIT, A. ENQVIST, and L. PÁL, "A Note on the Multiplicity Expressions in Nuclear Safeguards," *Nucl. Instrum. Meth. Phys. Res. A*, **603**, *3*, 541 (2009); https://doi.org/10.1016/j.nima.2009.03.018.
11. K. M. CASE, F. DE HOFFMANN, and G. PLACZEK, *Introduction to the Theory of Neutron Diffusion*, Vol. I, Los Alamos Scientific Laboratory (1953); https://books.google.se/books?id=ftJWAAAAMAAJ (current as of July 3, 2021).
12. G. I. BELL and S. GLASSTONE, *Nuclear Reactor Theory*, Van Nostrand Reinhold Company, New York (1970).
13. M. M. R. WILLIAMS, *Mathematical Methods in Particle Transport Theory*, Butterworths, London (1971).

14. I. CARLVIK, "Collision Probabilities for Finite Cylinders and Cuboids," *Nucl. Sci. Eng.*, **30**, *1*, 150 (1967); https://doi.org/10.13182/NSE30-01-150TN.

15. I. PÁZSIT, L. PÁL, and A. ENQVIST, "Böhnel Multiplicity Formulae Beyond the Point Model," *Proc. Int. Conf. Mathematics and Computational Methods Applied to Nuclear Science and Engineering (M&C 2019)*, Portland, Oregon, August 25–29, 2019, American Nuclear Society (2019).

16. H. VAN DAM, "Letter to the Editor," *Ann. Nucl. Energy*, **29**, *9*, 1137 (2002); https://doi.org/10.1016/S0306-4549(01)00119-0.

17. V. ARZHANOV, "Monotonicity Properties of k_{eff} with Shape Change and with Nesting," *Ann. Nucl. Energy*, **29**, *2*, 137 (2002); https://doi.org/10.1016/S0306-4549(01)00032-9.

18. A. ENQVIST, I. PÁZSIT, and S. AVDIC, "Sample Characterization Using Both Neutron and Gamma Multiplicities," *Nucl. Instrum. Meth. Phys. Res. A*, **615**, *1*, 62 (2010); https://doi.org/10.1016/J.Nima.2010.01.022.